RSC Advances

PAPER

View Article Online
View Journal | View Issue

Cite this: *RSC Adv.*, 2020, **10**, 18560

$CuZn_2InTe_4$ quantum dots-a novel nanostructure employing a green synthesis route†

Libin Kuriakose, N. J. Simi and V. V. Ison *

Received 2nd April 2020
Accepted 4th May 2020

DOI: 10.1039/d0ra02980g

rsc.li/rsc-advances

We report the synthesis and characterisation of novel $CuZn_2InTe_4$ quantum dots (QDs) suitable for various optoelectronic applications. The nanostructures grown are technologically important due to their Cd and Pb-free composition. The synthesis was maintained "green" by using a phosphine free organometallic procedure utilizing octadecene as the coordinating solvent. The structural properties of the nanocrystals (NCs) were analyzed using high resolution transmission electron microscopy (HRTEM), selected area electron diffraction (SAED) and X-ray diffraction (XRD). The composition was verified using X-ray photoelectron spectroscopy (XPS), inductive coupled plasma-optical emission spectroscopy (ICP-OES) and energy dispersive X-ray spectroscopy (EDX). The optical studies were performed using UV-VIS-NIR spectroscopy and photoluminescence (PL) spectroscopy and the band gap value obtained was verified using cyclic voltammetry (CV). The nanostructures grown were spherical with a size of about 5 nm possessing appreciable monodispersity.

Introduction

Semiconductor nanoparticles or quantum dots (QDs) have been the centre of attraction of materials research during the past few decades due to their potential applications in solar cells,[1–4] light emitting diodes,[5–8] imaging applications,[9,10] *etc.* Their unique properties like tuneable energy bandgap make them ideal for using in the visible and near infrared regions of the electromagnetic spectrum.[11–14] Among the variety of QDs explored, the most extensively studied systems are the Cd and Pb based chalcogenide QDs, which have their own advantages and disadvantages.[15–17] Different synthesis options like the colloidal organometallic hot injection method,[15,18] precursor decomposition method,[19] solvothermal method,[20] solid-state reaction,[21] thermolysis,[22] *etc.* have been adopted for the growth of these nanostructures with varying levels of success. The colloidal hot injection technique, introduced by Murray *et al.* and Peng *et al.* and later by Talapin *et al.* stands best in this sequence because of its features like the nanostructures synthesized have uniformity in size and shape, sharp absorption and emission peak, surface passivation capabilities, *etc.*[15,23–27] Colloidal techniques involve dissolving part of the semiconductor precursors in coordinating solvents held at high temperature and injecting the remaining part dissolved in suitable solvents swiftly into the first at a same or a lower temperature. The precursors dissociate and coalesce to nucleate the crystal growth. The coordinating ligands adhere to the growing crystal, reducing the number of available sites for further crystal growth and act to moderate and control the growth of the crystal.[15,24,28–30]

A critical analysis of the research literature shows that most of the synthesis procedures reported are based on toxic organophosphines[16,31] and developing green[28,31–36] initiatives is a major concern of the present day research community. Also, synthesizing QDs devoid of Cd and Pb is another thrust area of materials research for future technologies.[12] In this regard, chalcogen based ternary and quaternary nanocomposites of I, II, and III groups stands as a strong choice against the Pb and Cd based QDs. In addition to the size and shape dependent optical properties,[37] these materials possess additional flexibilities in tuning the emission peaks by various ways like varying stoichiometric ratios of chemical components,[38] optimizing growth time[39] and injection temperature,[16] *etc.*[12,14] Obviously, there will be more degrees of freedom in tuning of emission properties in quaternary components than ternary ones. Also, in these materials, the emission also arises from trap states rather than the excitonic emission.[14,40]

CuInSeS is an important quaternary QD system that has been developed for light harvesting applications.[11] Less toxic CuZnInS QDs with tuneable emission is another material explored for various opto-electronic applications.[12] Cu doped Zn–In–Se nanocrystals with appreciable quantum yield has been reported by different research groups.[36,41] Quaternary nanocrystals of $Cu_2ZnSnTe_4$ with metallic-like conduction and $Ag_2ZnSnSe_4$ with polaronic-type conduction, prepared using colloidal methods, have been explored for potential thermoelectric applications.[42,43] Recently, quaternary chalcogenide systems such as $CuZn_2InTe_4$, $CuMn_2InTe_4$ and $AgZn_2InTe_4$, with an electronic

Centre for Nano Bio Polymer Science and Technology, Department of Physics, St. Thomas College, Palai, Arunapuram, Kottayam, 686574, Kerala, India. E-mail: isonv@rediffmail.com; Tel: +919446126926

† Electronic supplementary information (ESI) available. See DOI: 10.1039/d0ra02980g

direct bandgap around 1 eV, has been reported in the bulk regime with a cubic zinc blende structure.[44–47]

In this study, we report the synthesis and characterization of novel quaternary Cu doped Zn–In–Te QDs with the composition $CuZn_2InTe_4$. The QDs were synthesised *via* green routes[31,33–36] by employing a heterogeneous suspension of Te in octadecene (ODE) and oleylamine (OLA) as the Te green precursor and dodecanethiol (DDT) as the capping ligand. To the best of our knowledge, this system has not yet been reported in the nano regime before. The nanostructures grown were characterized using high resolution transmission electron microscopy (HRTEM), selected area electron diffraction (SAED), X-ray diffraction (XRD), X-ray photoelectron spectroscopy (XPS), inductive coupled plasma optical emission spectroscopy (ICP-OES), energy dispersive X-ray spectroscopy (EDX), optical absorption, photoluminescence (PL) and cyclic voltammetry (CV) studies.

Experimental

Materials and methods

Copper(I) chloride (CuCl, anhydrous, beads, ≥99.99% trace metals basis), indium(III) acetate ($In(Ac)_3$, 99.99% trace metals basis), zinc acetate ($Zn(Ac)_2$, 99.99% trace metals basis), tellurium powder (Te, 200 mesh, 99.99%), 1-octadecene (ODE, technical grade, 90%), 1-dodecanethiol (DDT, ≥98%), oleylamine (OLA, technical grade, 70%) and tetrabutylammonium hexafluorophosphate ($TBAPF_6$, 98%) were purchased from Sigma-Aldrich. The chemicals were used as such without further purification.

Preparation of Te-suspension

The tellurium suspension (Te-SUS) was prepared by dispersing 1 mmol (128 mg) of Te powder in mixture of 2 ml of ODE and 1 ml of OLA. To make the suspension uniform, it was sonicated for 5 minutes without heating.

Synthesis of $CuZn_2InTe_4$

In a typical synthesis, CuCl (6 mg, 0.06 mmol), $In(Ac)_3$ (88 mg, 0.3 mmol), $Zn(Ac)_2$ (55 mg, 0.3 mmol), DDT (1 ml), OLA (1 ml) and ODE (5 ml) were taken in a three necked 100 ml round bottom (RB) flask and was then degassed for 20 minutes and heated to 100 °C in an inert (Ar) atmosphere. After removing the water vapour, if any, present, the mixture was slowly heated to 200 °C to make it a clear homogeneous solution. At this temperature, the Te-SUS was swiftly injected into it to initiate the growth of the $CuZn_2InTe_4$ QDs and the mixture was retained at 200 °C for another 20 minutes. After that, the solution was cooled down to room temperature suddenly. The QDs were purified using chloroform and methanol, precipitated using acetone and were finally dispersed in chloroform for further studies.

Characterisation of $CuZn_2InTe_4$

The HRTEM images of the samples were recorded using JEOL JEM-2100, 200 kV analytical electron microscope, accompanied by SAED, after depositing the QDs on carbon coated copper grids. The powder XRD studies were carried out using a Rigaku miniflex X-ray diffractometer using CuK_α ($\lambda = 1.54056$ Å) radiation. The XPS studies were performed on a PHI 5000 VersaProbe scanning ESCA (electron spectroscopy for chemical analysis) microprobe. The ICP-OES studies were carried out using a PerkinElmer Optima 5300 DV system. EDX studies were performed using a JEOL JED-2300 analysis station attached to the JEM-2100 microscope. The optical absorption was analyzed using a Shimadzu-3600 UV-VIS-NIR spectrophotometer and the PL spectrum was recorded using a Horiba, FluoroMax-4, compact spectrofluorometer. CV studies were done on a Metrohm Autolab 204N electrochemical workstation.

Results and discussion

The HRTEM image of the QDs is shown in Fig. 1. The image indicates that the nanostructures grown are spherical with an average diameter of 5 ± 0.5 nm possessing appreciable monodispersity. The image shows no signs of agglomeration. The interplanar spacing of 0.33 nm is attributed to the (111) plane that matches with the SAED pattern shown in the inset. The results obtained using HRTEM and SAED are in good agreement with the XRD data, to be discussed later.

XPS was used to confirm the composition of the nanostructures employing AlK_α source with energy 1486.6 eV, operating at 49.8 W, for a 200 micron beam size. A pass energy of 46.95 eV was used to acquire the high-resolution spectra. The spectra were charge-corrected with reference to the C 1s signal (283.4 eV). The XPS survey spectrum of QDs is provided in ESI (Fig. S1).† The XPS spectra corresponding to Cu, In, Zn and Te are shown in Fig. 2.

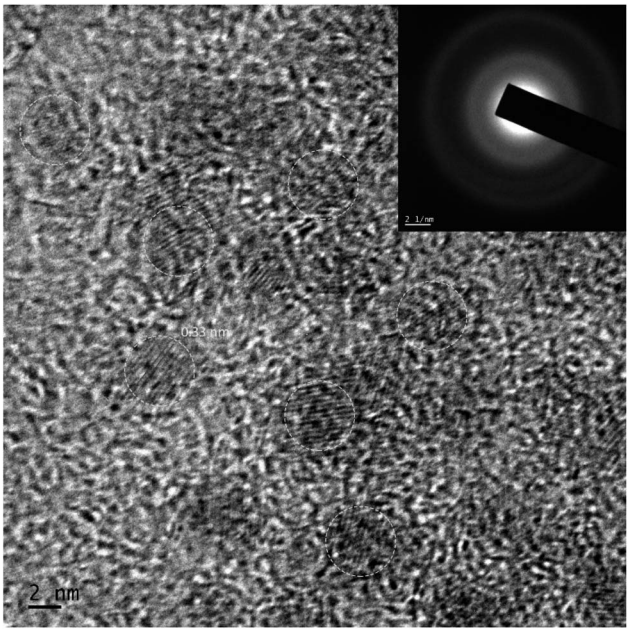

Fig. 1 HRTEM image of Cu doped Zn–In–Te. Inset shows the SAED pattern of the same.

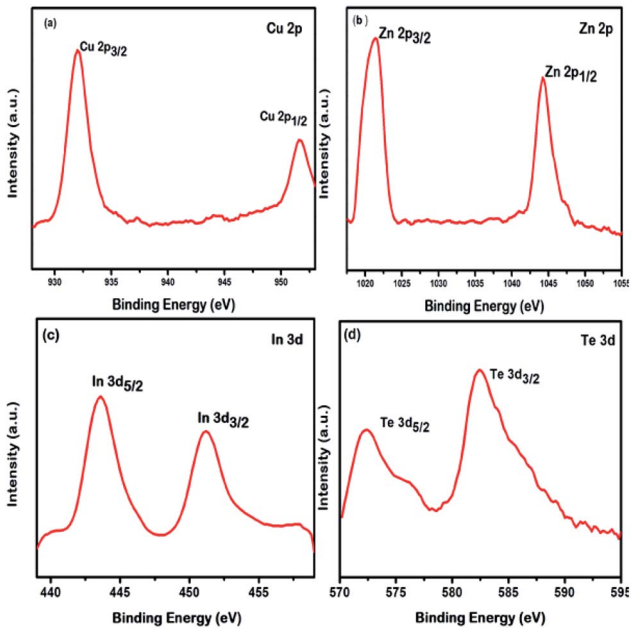

Fig. 2 XPS Spectra of Cu doped Zn–In–Te. (a) Cu 2p (b) Zn 2p (c) In 3d and (d) Te 3d.

An oxidation state of +1 can be assigned to Cu from the position of its energy states $2p_{3/2}$ (933.4 eV) and $2p_{1/2}$ (953.0 eV) with a spin orbit separation 19.6 eV and the Cu LMM auger level.[48–50] The energy levels $2p_{3/2}$ and $2p_{1/2}$ positioned at 1023.0 eV and 1045.6 eV, respectively, separated by 22.6 eV and its LMM auger level indicates a +2 oxidation state for Zn.[51,52] An MNN auger level along with the $3d_{3/2}$ level at 452.8 eV and $3d_{5/2}$ at 444.6 eV, separated by 8.2 eV is indicative of a +3 oxidation state for In.[53,54] The Te energy levels $3d_{5/2}$ at 573.4 eV and $3d_{3/2}$ at 583.4 eV, with a spin orbit separation 10 eV and the MNN auger level suggests a −2 oxidation state for Te.[55,56] The valence states Cu^{+}, Zn^{2+}, In^{3+} and Te^{2-} confirms the composition of the Cu doped Zn–In–Te as $CuZn_2InTe_4$.

The composition of the QDs was further confirmed by ICP-OES with the help of an acid digestion method and the result obtained is shown in Table 1. The data confirms the presence of Cu, Zn, In, and Te. The atomic ratio Cu : Zn : In : Te comes out to be 1.00 : 2.26 : 1.15 : 3.87, which is in good agreement with the stoichiometry of $CuZn_2InTe_4$.

The elemental analysis was further carried out using EDX indicating the presence of the elements Cu, Zn, In, and Te and the spectrum obtained is shown in Fig. 3. The amount of Cu is a bit larger because of carbon-coated cupper TEM grids used.

Table 1 ICP-OES measurements of Cu–Zn–In–Te quantum dots

Element symbol	Wavelength (nm)	Concentration (mg L^{-1})
Cu	327.393	31.80
Zn	206.200	73.94
In	230.606	66.08
Te	214.281	247.25

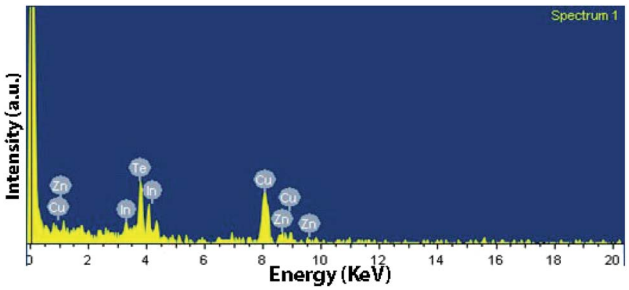

Fig. 3 EDX spectrum of $CuZn_2InTe_4$.

The XRD pattern of the nanostructures synthesized is shown in Fig. 4, having 3 major peaks corresponding to the (111), (220) and (311) planes of bulk $CuZn_2InTe_4$ with a cubic structure along with few minor peaks (ICDD 00-027-0161). The broadened peaks indicate nano-sized particles. D_{hkl}, the size of the QDs in a direction perpendicular to the lattice planes with Miller indices hkl is calculated using the Scherrer formula.[57,58]

$$D_{hkl} = K\lambda/(\beta_{hkl}\cos\theta)$$

where, K is a numerical factor referred to as the crystallite-shape factor, λ is the wavelength of the X-rays used, β_{hkl} is the full-width at half-maximum (FWHM) of the diffraction peak in radians and θ is the Bragg angle. The results obtained matches well with the HRTEM data.

ESI (Fig. S2)† shows the absorption spectra of the QDs dispersed in chloroform. The optical bandgap of $CuZn_2InTe_4$ QDs was calculated using the Tauc's relation,[59–61]

$$\alpha = (A/h\nu)(h\nu - E_g)^r$$

where, α is the optical absorption coefficient, A is a constant to associate the band tailing, $h\nu$ is the photo energy, E_g is the bandgap of the material and the exponent r represent the nature of transition. We have obtained a bandgap of 1.816 eV by

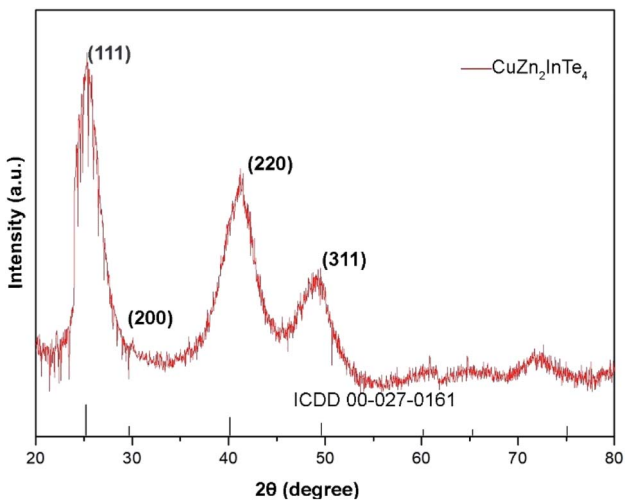

Fig. 4 XRD pattern of $CuZn_2InTe_4$.

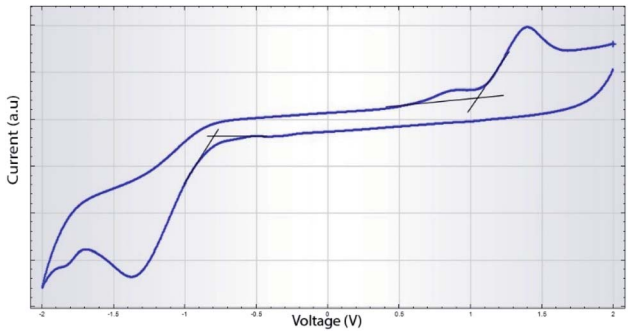

Fig. 5 Cyclic voltammograms of $CuZn_2InTe_4$.

extrapolating the linear region of the obtained curve to abscissa as shown in ESI (Fig. S3).† Photoluminescence (PL) spectrum of $CuZn_2InTe_4$ QDs is shown in ESI (Fig. S4).†

The CV measurements were performed using glassy carbon as the working electrode, a platinum wire as the counter electrode and Ag/Ag^+ (0.01 M) as the reference electrode. A 0.1 M solution of tetrabutylammonium hexafluorophosphate ($TBAPF_6$) in acetonitrile was used as the supporting electrolyte. The QDs dispersed in chloroform was deposited on to the glassy carbon electrode after proper polishing and cleaning of it. A scan rate of 50 mV s^{-1} was maintained during the CV studies. The cyclic voltammograms are shown in Fig. 5. The HOMO and LUMO energy levels of the QDs can be obtained from the oxidation and reduction potentials with respect to the potential of the reference electrode and are given by[36,62,63]

$$E_{HOMO} = -(E^{OX} + 4.71)\ eV$$

$$E_{LUMO} = -(E^{RED} + 4.71)\ eV$$

where E^{OX} stands for the onset of the oxidation potential and E^{RED} the corresponding reduction potential. From the E^{OX} (1.05 V) and E^{RED} (−0.8 V), the HOMO and LUMO levels can be obtained as −5.76 eV and −3.91 eV respectively, giving a bandgap of 1.85 eV. This value is in close agreement with the value obtained from the optical absorption measurements.

Conclusions

Novel $CuZn_2InTe_4$ QDs were synthesised *via* green route in a phosphine free environment. The nanostructures grown were spherical and monodisperse with well-defined lattice planes as suggested by HRTEM imaging and SAED pattern. The chemical composition was confirmed using XPS, ICP-OES and EDX studies. The structural information was gathered from XRD analysis indicating a cubic structure. The optical bandgap measured from optical absorption was found to be in close agreement with the electrochemical bandgap obtained from CV measurements.

Conflicts of interest

There are no conflicts to declare.

References

1 T. Torimoto, T. Kameyama and S. Kuwabata, *J. Phys. Chem. Lett.*, 2014, **5**, 336–347.
2 S. E. Lohse and C. J. Murphy, *J. Am. Chem. Soc.*, 2012, **134**, 15607–15620.
3 S. V. Kershaw, A. S. Susha and A. L. Rogach, *Chem. Soc. Rev.*, 2013, **42**, 3033–3087.
4 J. Wang, I. Mora-Seró, Z. Pan, K. Zhao, H. Zhang, Y. Feng, G. Yang, X. Zhong and J. Bisquert, *J. Am. Chem. Soc.*, 2013, **135**, 15913–15922.
5 W. Zhang, Q. Lou, W. Ji, J. Zhao and X. Zhong, *Chem. Mater.*, 2014, **26**, 1204–1212.
6 I. S. Sohn, S. Unithrattil and W. B. Im, *ACS Appl. Mater. Interfaces*, 2014, **6**, 5744–5748.
7 A. E. Ahmed Nabawy Morra, W. M. Swelm and A. E.-S. Abou El-Azm, *Opt. Quantum Electron.*, 2011, **42**, 285–296.
8 D. V. Talapin, J.-S. Lee, M. V. Kovalenko and E. V. Shevchenko, *Chem. Rev.*, 2010, **110**, 389–458.
9 M. F. Foda, L. Huang, F. Shao and H.-Y. Han, *ACS Appl. Mater. Interfaces*, 2014, **6**, 2011–2017.
10 P. Zrazhevskiy, M. Sena and X. Gao, *Chem. Soc. Rev.*, 2010, **39**, 4326–4354.
11 H. McDaniel, A. Y. Koposov, S. Draguta, N. S. Makarov, J. M. Pietryga and V. I. Klimov, *J. Phys. Chem. C*, 2014, **118**, 16987–16994.
12 W. Zhang, Q. Lou, W. Ji, J. Zhao and X. Zhong, *Chem. Mater.*, 2014, **26**, 1204–1212.
13 D. Pan, D. Weng, X. Wang, Q. Xiao, W. Chen, C. Xu, Z. Yang and Y. Lu, *Chem. Commun.*, 2009, 4221–4223.
14 T. Jiang, J. Song, H. Wang, X. Ye, H. Wang, W. Zhang, M. Yang, R. Xia, L. Zhu and X. Xu, *J. Mater. Chem. B*, 2015, **3**, 2402–2410.
15 C. B. Murray, D. J. Norris and M. G. Bawendi, *J. Am. Chem. Soc.*, 1993, **115**, 8706–8715.
16 S. Cingarapu, Z. Yang, C. M. Sorensen and K. J. Klabunde, *J. Nanomater.*, 2012, **2012**, 12.
17 H. Choi, J. H. Song, J. Jang, X. D. Mai, S. Kim and S. Jeong, *Nanoscale*, 2015, **7**, 17473–17481.
18 H. Zhong, Y. Li, M. Ye, Z. Zhu, Y. Zhou, C. Yang and Y. Li, *Nanotechnology*, 2006, **18**, 025602.
19 I. Tsuyumoto, T. Kato and T. Arai, *Mater. Res. Bull.*, 2010, **45**, 1899–1902.
20 B. Li, Y. Xie, J. Huang and Y. Qian, *Adv. Mater.*, 1999, **11**, 1456–1459.
21 K. Yoshino, T. Ikari, S. Shirakata, H. Miyake and K. Hiramatsu, *Appl. Phys. Lett.*, 2001, **78**, 742–744.
22 S. L. Castro, S. G. Bailey, R. P. Raffaelle, K. K. Banger and A. F. Hepp, *Chem. Mater.*, 2003, **15**, 3142–3147.
23 C. B. Murray, M. Nirmal, D. J. Norris and M. G. Bawendi, *Z. Physik D Atoms, Mol. Clust.*, 1993, **26**, 231–233.
24 X. Peng, J. Wickham and A. P. Alivisatos, *J. Am. Chem. Soc.*, 1998, **120**, 5343–5344.
25 X. Peng, L. Manna, W. Yang, J. Wickham, E. Scher, A. Kadavanich and A. P. Alivisatos, *Nature*, 2000, **404**, 59–61.
26 D. V. Talapin, A. L. Rogach, A. Kornowski, M. Haase and H. Weller, *Nano Lett.*, 2001, **1**, 207–211.

27 Y. Pu, F. Cai, D. Wang, J.-X. Wang and J.-F. Chen, *Ind. Eng. Chem. Res.*, 2018, **57**, 1790–1802.
28 C. A. M. Bonilla and V. V. Kouznetsov, *Green Nanotechnology*, IntechOpen, Rijeka, 2016, ch. 7.
29 D. J. Norris, A. L. Efros and S. C. Erwin, *Science*, 2008, **319**, 1776–1779.
30 M. I. Bodnarchuk and M. V. Kovalenko, *Engineering colloidal quantum dots*, ed. G. Konstantatos and E. H. Sargent, Cambridge University Press, 2013, pp. 1–29.
31 C. Bullen, J. van Embden, J. Jasieniak, J. E. Cosgriff, R. J. Mulder, E. Rizzardo, M. Gu and C. L. Raston, *Chem. Mater.*, 2010, **22**, 4135–4143.
32 X. Peng, *Chem.–Eur. J.*, 2002, **8**, 334–339.
33 C. Pu, J. Zhou, R. Lai, Y. Niu, W. Nan and X. Peng, *Nano Res.*, 2013, **6**, 652–670.
34 J. Z. Niu, H. Shen, H. Wang, W. Xu, S. Lou, Z. Du and L. S. Li, *New J. Chem.*, 2009, **33**, 2114–2119.
35 J. Jasieniak, C. Bullen, J. van Embden and P. Mulvaney, *J. Phys. Chem. B*, 2005, **109**, 20665–20668.
36 S. Cao, W. Ji, J. Zhao, W. Yang, C. Li and J. Zheng, *J. Mater. Chem. C*, 2016, **4**, 581–588.
37 C. d. M. Donegá, *Chem. Soc. Rev.*, 2011, **40**, 1512–1546.
38 J. Q. Grim, L. Manna and I. Moreels, *Chem. Soc. Rev.*, 2015, **44**, 5897–5914.
39 J. T. Siy, E. H. Brauser, T. K. Thompson and M. H. Bartl, *J. Mater. Chem. C*, 2014, **2**, 675–682.
40 B. Mao, C.-H. Chuang, J. Wang and C. Burda, *J. Phys. Chem. C*, 2011, **115**, 8945–8954.
41 J. Ke, X. Li, Q. Zhao, Y. Shi and G. Chen, *Nanoscale*, 2014, **6**, 3403–3409.
42 K. Wei and G. S. Nolas, *ACS Appl. Mater. Interfaces*, 2015, **7**, 9752–9757.
43 K. Wei and G. S. Nolas, *J. Solid State Chem.*, 2015, **226**, 215–218.
44 D. Hobbis, W. Shi, A. Popescu, K. Wei, R. E. Baumbach, H. Wang, L. M. Woods and G. S. Nolas, *Dalton Trans.*, 2020, **49**, 2273–2279.
45 W. Shi, A. R. Khabibullin, D. Hobbis, G. S. Nolas and L. M. Woods, *J. Appl. Phys.*, 2019, **125**, 155101.
46 D. Hobbis, K. Wei, H. Wang and G. S. Nolas, *J. Alloys Compd.*, 2018, **743**, 543–546.
47 G. S. Nolas, M. S. Hassan, Y. Dong and J. Martin, *J. Solid State Chem.*, 2016, **242**, 50–54.
48 M. C. Biesinger, *Surf. Interface Anal.*, 2017, **49**, 1325–1334.
49 M. C. Biesinger, L. W. Lau, A. R. Gerson and R. S. Smart, *Appl. Surf. Sci.*, 2010, **257**, 887–898.
50 M.-Y. Chiang, S.-H. Chang, C.-Y. Chen, F.-W. Yuan and H.-Y. Tuan, *J. Phys. Chem. C*, 2011, **115**, 1592–1599.
51 H. Shen, H. Yuan, F. Wu, X. Bai, C. Zhou, H. Wang, T. Lu, Z. Qin, L. Ma and L. S. Li, *J. Mater. Chem.*, 2012, **22**, 18623–18630.
52 S. D. Perera, H. Zhang, X. Ding, A. Nelson and R. D. Robinson, *J. Mater. Chem. C*, 2015, **3**, 1044–1055.
53 C. Bullen, J. van Embden, J. Jasieniak, J. E. Cosgriff, R. J. Mulder, E. Rizzardo, M. Gu and C. L. Raston, *Chem. Mater.*, 2010, **22**, 4135–4143.
54 Y. Chen, S. Li, L. Huang and D. Pan, *Inorg. Chem.*, 2013, **52**, 7819–7821.
55 C. Han, Z. Li, W.-j. Li, S.-l. Chou and S.-x. Dou, *J. Mater. Chem. A*, 2014, **2**, 11683–11690.
56 A. C. Poulose, S. Veeranarayanan, M. S. Mohamed, R. R. Aburto, T. Mitcham, R. R. Bouchard, P. M. Ajayan, Y. Sakamoto, T. Maekawa and D. S. Kumar, *Sci. Rep.*, 2016, **6**, 35961.
57 P. Scherrer, *Mathematisch-Physikalische Klasse*, 1918, vol. 2, pp. 98–100.
58 U. Holzwarth and N. Gibson, *Nat. Nanotechnol.*, 2011, **6**, 534.
59 J. Tauc, *Mater. Res. Bull.*, 1968, **3**, 37–46.
60 E. A. Davis and N. F. Mott, *Philos. Mag.*, 1970, **22**, 0903–0922.
61 D. L. Wood and J. Tauc, *Phys. Rev. B*, 1972, **5**, 3144–3151.
62 H. Zhong, S. S. Lo, T. Mirkovic, Y. Li, Y. Ding, Y. Li and G. D. Scholes, *ACS Nano*, 2010, **4**, 5253–5262.
63 Y. Yang, H. Zhong, Z. Bai, B. Zou, Y. Li and G. D. Scholes, *J. Phys. Chem. C*, 2012, **116**, 7280–7286.